Robot Catching with High Manipulability Grasp Configuration using Vision

Tasuku Yamawaki, Shiro Asano, Hideyuki Miyashita and Masahito Yashima
Dept. of Mechanical Systems Engineering
National Defense Academy of Japan
1-10-20, Hashirimizu, Yokosuka, Kanagawa, Japan
{*yamawaki & yashima*}*@nda.ac.jp*

***Abstract*—The present paper proposes the strategy for a robotic hand to catch a free-flying object with a high manipulability grasp configuration. Several researchers have succeeded in catching the free-frying object by the robotic hand. However, these researches focus on only the catching and do not discuss the grasp configuration after the catching. It is important to consider not only the stable catching but also the following manipulation after the catching as seen in a juggling and a baton twirling. We propose the strategy that enables the robotic hand to catch the object with a high manipulability grasp configuration and verify the proposed strategy experimentally by using the newly developed three-fingered hand.**

***Index Terms*—Robot catching, Robotic hand, Thumb opposability, Pre-shaping**

I. Introduction

The present paper proposes the strategy for a robotic hand to catch the free-flying object with a high manipulability grasp configuration.

A grasping algorithm has been studied by many researchers [1], [6], [10]. These grasping algorithms deal with a stationary object. On the other hand, the present paper discusses a grasping task of a moving object, such as the robot catching of the free-flying ball as shown in Fig. 1.

There have been several researches which succeed in catching a moving object, which utilize model based prediction methods to predict the path of a tossed ball [3] and the high-speed visual servo [8]. These researches focus on the development of the algorithm of the visual feedback control and take no account of its grasp configuration of the robotic hand. The robotic hand with such grasp configuration is hard to accomplish a juggling and a baton twirling which require starting the dexterous manipulation just after the catching. Taking account of the following manipulation after the catching, the present paper proposes the catching strategy which enables the robotic hand to catch the object with a high manipulability configuration, and verify its validity experimentally. Although there is work on the robot catching with the grasp configuration given in advance [9], the importance of the selection of the grasp configuration after the catching has not been discussed.

At first, we describe the newly developed three-fingered hand, the NDA Hand, in Section II, which was applied to the catching experiment. In Section III, we show the catching strategy which enables the robotic hand to catch the free-flying object with a high manipulability grasp configuration in a vertical plane. In order to obtain the high manipulability configuration, the derivation of the manipulability measure of a robotic hand is also shown. Finally, in Section IV, we verify the proposed strategy by experiments on catching a ball after bouncing on a table using a high speed camera and the NDA Hand as shown in Fig. 1.

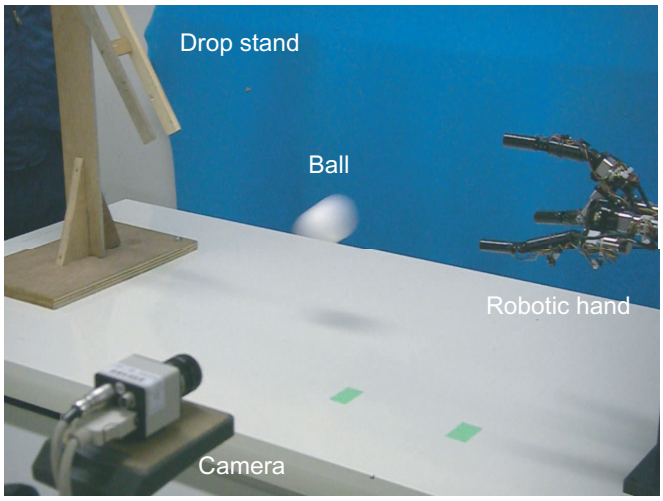

Fig. 1. Experimental set-up of the robot catching using vision

II. Robotic Hand

A. Design and Performance

Fig. 2 shows a photo of the robotic hand (the NDA Hand) we developed in our laboratory, which is applied to the robot catching. Fig. 3 shows the hand model. The hand is almost the same size as an adult's hand and weighs about 600 g. To manipulate an object to arbitrary position and orientation by the hand, each finger is required having 3 DOF at least [2]. The NDA hand consists of three of 3 DOF finger with a built-in actuator. The three joints of each finger are labeled as joint 1, 2, and 3 from the finger base. The rotational axis of the joint 1 of the finger 1 tilts 30 degrees from the z-axis.

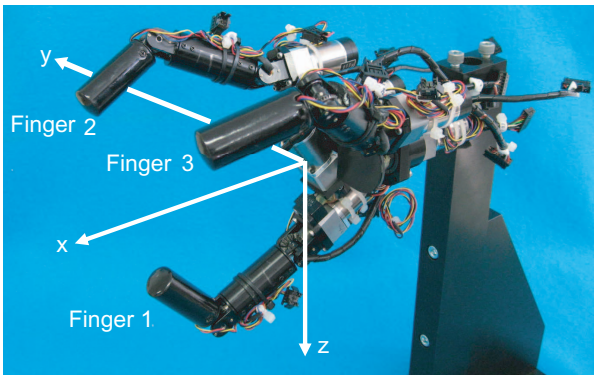

Fig. 2. The NDA Hand

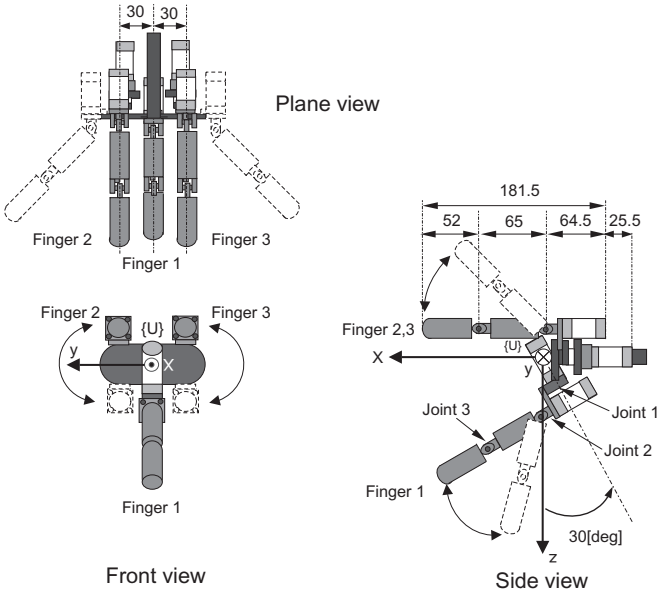

Fig. 3. Robotic hand mechanism

Conversely, the rotational axis of the joint 1 of the finger 2 and 3 are set parallel to the x-axis. These finger arrangements enable the robotic hand to achieve a finger-thumb opposition, which is shown in the next section.

A newly developed high-power mini actuator with a small harmonic drive gear by the Harmonic Drive Systems Inc. are fitted in each finger link to achieve light weight and high speed performance. The hand achieves maximum high-speed motion of 5.1 m/s and high power of 28.5 N at the fingertip. The joint 1, which has the maximum moment of inertia, can track the 5.5 Hz sine wave without delay and can rapidly reach 180 deg within about 0.3 sec.

B. Finger-Thumb Opposition

A human hand has ability to grasp objects with various shapes by numerous grasp configurations. The finger-thumb opposition (Fig. 4) enables a human hand to gain such adaptability [7], whose characteristics are described as follows:

Fig. 4. Finger-Thumb Opposition

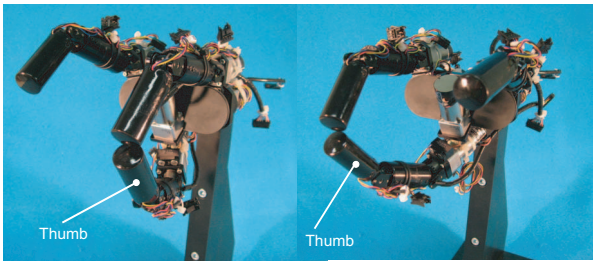

Fig. 5. Thumb opposability of robotic hand

a) The first joint of thumb has the rotational axis which is almost vertical to the first joint of the other fingers. This yields the opposition between the thumb and the other fingers.
b) The opening between the thumb and the index finger is large. This yields the adaptation to objects with various sizes.

As shown in Fig. 5, the NDA Hand achieves the finger-thumb opposition. The finger 1 functions as the thumb and can be opposed to the finger 2 and 3. For the robot catching, the finger-thumb opposition provides a wide catching area. This gives the robotic hand robustness against the trajectory change of the free-flying object.

III. Catching Strategy

This section discusses the strategy of the robot catching as shown in Fig. 6. To simplify the problem, it is assumed that the ball remains in the vertical plane. The manipulability measure of a robotic hand is also derived to plan a catching configuration with a high manipulability grasp.

A. Three Phases of Robot Catching

We divide the robot catching into three phases according as the horizontal position where the ball passes, which are denoted by the line 1, 2 and 3, as shown in Fig. 6. The three phases are called the standby phase, the pre-shaping phase and the catching phase, respectively. The procedure of setting the position of the line 1, 2 and 3 are described in section IV-B3. We describe below the each phase in detail.

Standby Phase: On the standby phase, the robotic hand keeps the standby configuration, which is discussed in section IV-B2, until the ball crosses the line 1. The line 1 is the trigger point to start the next pre-shaping phase.

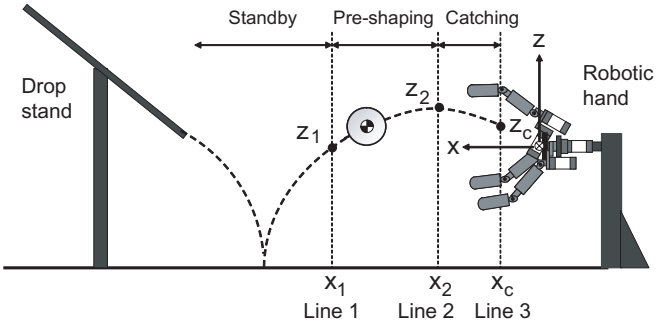

Fig. 6. Catching strategy

Pre-shaping Phase:

When a human being grasps an object, a human hand forms the pre-grasp configuration in advance to grasp the object easily as shown in Fig. 7, which is known as a pre-shaping [4]. We apply the concept of the pre-shaping to the robot catching.

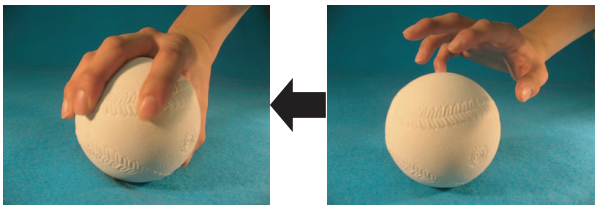

Fig. 7. A pre-shaping for a ball

At the moment when the ball crosses the line 1, we measure the height of the ball z_1 with a high-speed camera, which is used as an initial prospective catching point on the line 3. At the same time, the robot hand starts the pre-shaping to form the high manipulability grasp configuration at the prospective catching point. The derivation of the high manipulability grasp configuration is described in section IV-B1. The novel manipulability measure is discussed in section III-B.

Catching Phase: To update the height of the prospective catching point, the line 2 is newly set. At the moment when the ball crosses the line 2, we re-measure the height of the ball z_2 with the high-speed camera and update the height of the prospective catching point to the height z_2. The robot hand restarts to form the high manipulability configuration of the updated catching point and completes the catching.

B. Manipulability of Robotic Hand

When the ball is caught by the robotic hand, the grasp configuration achieving the high manipulability is selected. To obtain high manipulability grasp configuration, we derive the manipulability measure of the robotic hand.

Assuming that sliding does not occur at any contact points, the velocity constraints between the velocity of the object $\boldsymbol{V}_O$ and the joint angular velocity $\dot{\boldsymbol{\theta}}$ can be described as

$$\begin{bmatrix} \boldsymbol{G}^T & -\boldsymbol{J} \end{bmatrix} \begin{bmatrix} \boldsymbol{V}_o \\ \dot{\boldsymbol{\theta}} \end{bmatrix} = 0 \tag{1}$$

where $\boldsymbol{G}$ is the wrench matrix and $\boldsymbol{J}$ is the hand Jacobian. We define the matrix $\boldsymbol{C}$ of which the column vector is basis for the null space of the matrix $\begin{bmatrix} \boldsymbol{G}^T & -\boldsymbol{J} \end{bmatrix}$ and divide $\boldsymbol{C}$ into the two matrices such as $\boldsymbol{C} = \begin{bmatrix} \boldsymbol{C}_V^T & \boldsymbol{C}_\theta^T \end{bmatrix}^T$. Thus the $\boldsymbol{V}_O$ and $\dot{\boldsymbol{\theta}}$ which satisfies (1) is restricted as

$$\boldsymbol{V}_o = \boldsymbol{C}_V \boldsymbol{z} \tag{2}$$

$$\dot{\boldsymbol{\theta}} = \boldsymbol{C}_\theta \boldsymbol{z} \tag{3}$$

where $\boldsymbol{z}$ is an arbitrary vector.

The velocity of the object given by the normalized joint angular velocity $\|\dot{\boldsymbol{\theta}}\| \leq 1$ can be described as

$$\|\boldsymbol{V}_o\|^2 = d_1 \bar{z}_1^2 + d_2 \bar{z}_2^2 + \cdots + d_p \bar{z}_p^2 \tag{4}$$

where $\bar{z}_1, \ldots, \bar{z}_p$ are arbitrary variables and $d_1, \cdots, d_p$ are the eigenvalues of the matrix $\boldsymbol{Q}$ in (11). The detail derivation of (4) is described in Appendix.

From the above discussion, the set of the velocity of the object given by the set of the normalized joint angular velocity $\|\dot{\boldsymbol{\theta}}\| \leq 1$ can be expressed as an ellipsoid with the principal axes $(\sqrt{d_1}\bar{z}_1,\ \sqrt{d_2}\bar{z}_2,\ \ldots\ \sqrt{d_p}\bar{z}_p)^T$. In the present research, we define the manipulability measure σ as the minimum singular value d_p, which can be described as

$$\sigma = d_p \tag{5}$$

The minimum singular value d_p corresponds to the controllable maximum velocity of the object in any direction that can be produced by a unit joint angular velocity.

IV. Experiment of Robot Catching

A. Experimental Setup

Applying the catching strategy described in the previous section to the NDA Hand (Fig. 2), we conduct the experiment of the robot catching. As shown in Fig. 1, the NDA Hand catches the rebound rubber-ball (of which the diameter is 62 mm) dropped from the stand. Since the ball moves fast, where the ball reaches the maximum velocity 3 m/s just after the rebound, we need to measure the position of the ball with high sampling rate. We use the high-speed intelligent vision system (Hamamatsu Photonics K.K.), which can measure the position of the ball at the rate of 1 kHz. We apply the xPC target®, which is one of the MATLAB® tools, to the controller whose sampling rate is 1 kHz. The overall robot catching system is shown in Fig. 8.

B. Parameter Settings for Robot Catching

Before starting the robot catching, we need to set several parameters, which are the standby configuration, the high manipulability grasp configuration and the position of three lines 1, 2, and 3. This section obtains these parameters.

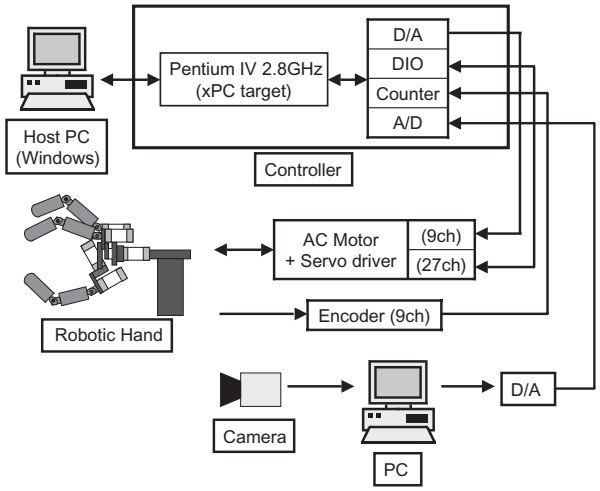

Fig. 8. Overall robot catching system

1) Precision Grasp Configuration: It is difficult to optimize the high manipulability grasp configuration in real time. Therefore, we prepared several candidates for catching points in the catchable area discretely, and obtain the high manipulability grasp configuration of each candidate in advance.

The high manipulability grasp configuration is decided to meet the following conditions, which are

a) The grasp configuration enables the robotic hand to catch the ball easily.
b) The grasp configuration enables the robotic hand to manipulate the ball easily after the catching.

As shown in Fig. 9, we prepare 21 candidates for catching points on the line 3 ($x_c = 0.07$ m), where the robotic hand gains the widest catchable range to the vertical direction. The candidates are set as 2 mm apart between $-0.02 \leq z_c \leq 0.02$ m, where the change of the joint angle can be small relatively.

If three contact points on the ball can be 120 degree apart on the ball's equator as shown in Fig. 10, the robotic hand gains the most stable grasp. We define this grasp configuration as the primary grasp configuration and obtain the high manipulability grasp configuration close to the primary grasp configuration.

To obtain such grasp configuration, we solve the mathematical programming described below.

$$\begin{aligned} &\text{minimize} && -\sigma \\ &\text{subject to} && u_o + 15 \geq 0, \quad -u_o + 15 \geq 0 \\ &&& v_o + 15 \geq 0, \quad -v_o + 15 \geq 0 \end{aligned}$$

where u_o and v_o respectively show the transitions of the latitude and the longitude on the ball from the contact point of the primary grasp configuration. By solving the above equations, we obtain the desired joint angle $\boldsymbol{\theta}^i_{goal} (i = 1, 2, \ldots, 21)$ at each candidate for catching point, where i indicates the number of the candidate for catching point.

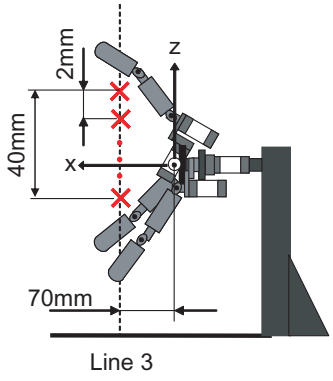

Fig. 9. The candidate for catching points

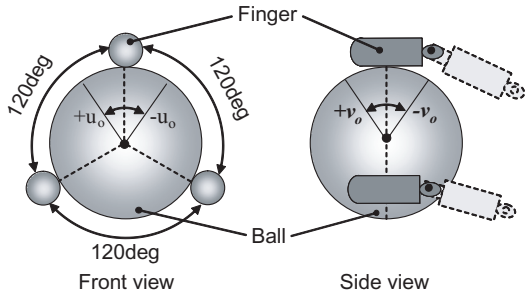

Fig. 10. A stable grasp configuration (the primary grasp configuration)

2) Standby Configuration: We set the standby configuration based on the following policies;

a) The standby configuration can be easily switched to any configuration.
b) The standby configuration should not be obstructive to the approaching ball.

From the first policy, we set the joint angle of the standby configuration $\boldsymbol{\theta}^i_{start}$ as the mean of the joint angle of the grasp configurations $\boldsymbol{\theta}^i_{goal}$. From the second policy, we add 30 degrees to the entire second joint to open the fingers.

3) Position of Line 1, 2 and 3: To set the position of the line 1, we have to consider

a) The response performance of the joint actuator
b) The velocity of the ball
c) The difference of joint angle between the standby configuration and the grasp configuration

At first, we obtain the maximum magnitude of the joint angular difference between the standby configuration and the grasp configuration. Thus the transition time from the standby configuration to the grasp configuration of the each joint can be obtained by utilizing the maximum joint angular velocity. We select the maximum transition time Δt_{max} among them and set the position of the line 1 as

$$x_1 = -v_x \Delta t_{max} + x_c \tag{6}$$

where $v_x < 0$ is the estimate of the horizontal velocity of the ball and $x_c = 0.07$ m is the position of the line 3. In this research, we set $x_1 = 0.33$ m.

The above strategy makes the transition time from the standby configuration to the grasp configuration smaller than the traveling time of the ball from line 1 to the catching point. This will yields the high successful rate of the robot catching.

We set the position of the line 2 as $x_2 = 0.15$ m heuristically, which produces the high successful rate. The line 3 indicates the horizontal position of the candidate for catching points. Thus the horizontal position of the line 3 is $x_c = 0.07$ m.

C. Experimental Results

The trajectory of the ball is described in Fig. 11, which is obtained by the high-speed camera. The solid line and the dashed line indicate the vertical position and the horizontal position of the ball, respectively. Although Fig. 11 shows the position of the ball does not change after 8.61 sec, the position of the ball after the time cannot be measured accurately because a part of the ball is hidden behind the fingers. From the captured picture recorded by the camcorder, the robotic hand caught the ball at $x = 0.075$ m, $z = -0.005$ m, which is close to the initial prospective catching points settled on the line 2 of which the height is $z_2 = -0.006$ m.

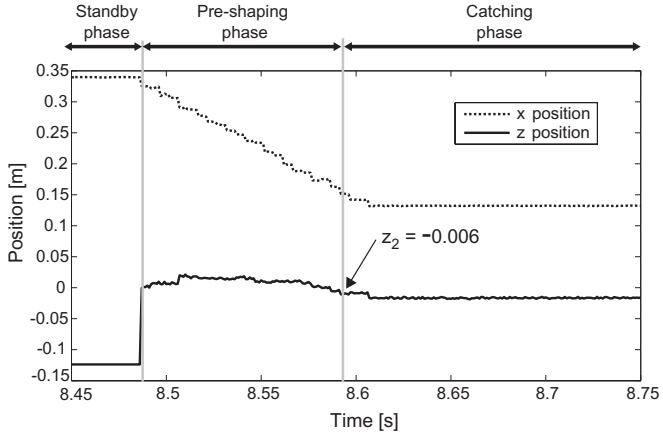

Fig. 11. Target position

The joint angles of all fingers are shown in Fig. 12. The angles of the joint 1, 2 and 3 are described by the solid line, the dashed-dotted line and the dotted line, respectively. All of the joints except the joint 1 of the finger 2 could reach the desired angle of the pre-shaping phase before the ball reached the line 2. The transition time of them is very short, which is less than 0.05 sec.

Fig. 13 shows the snapshots of the robot catching. The robot hand accomplished the catch of the flying-ball with the high manipulability grasp configuration. The success rate

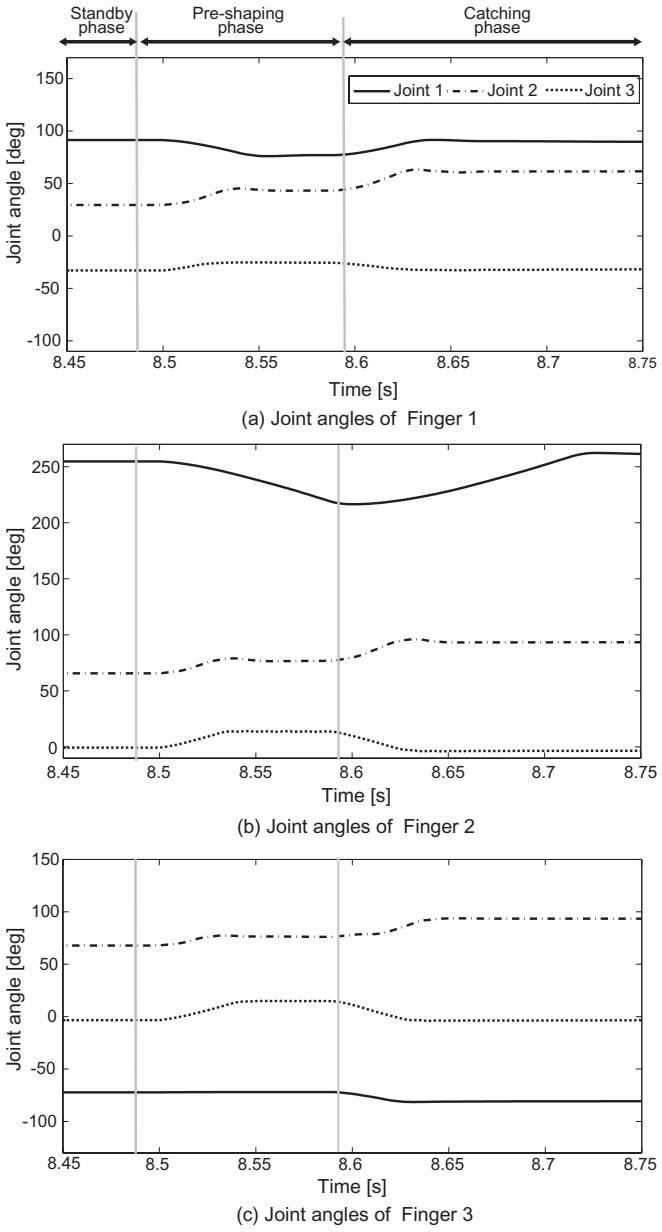

Fig. 12. Trajectory of joint angle

for the experiments was about 30%. The largest cause of the failure is that the trajectory of the rebound rubber-ball deviates from the vertical plane due to its elasticity and the friction between the rubber-ball and the ground.

Even if the shape or material of the object is changed, we can apply the present strategy by resetting the catching and standby configurations and the position of the line 1, 2 and 3 as shown in Section IV-B. Its experimental verification is our future work.

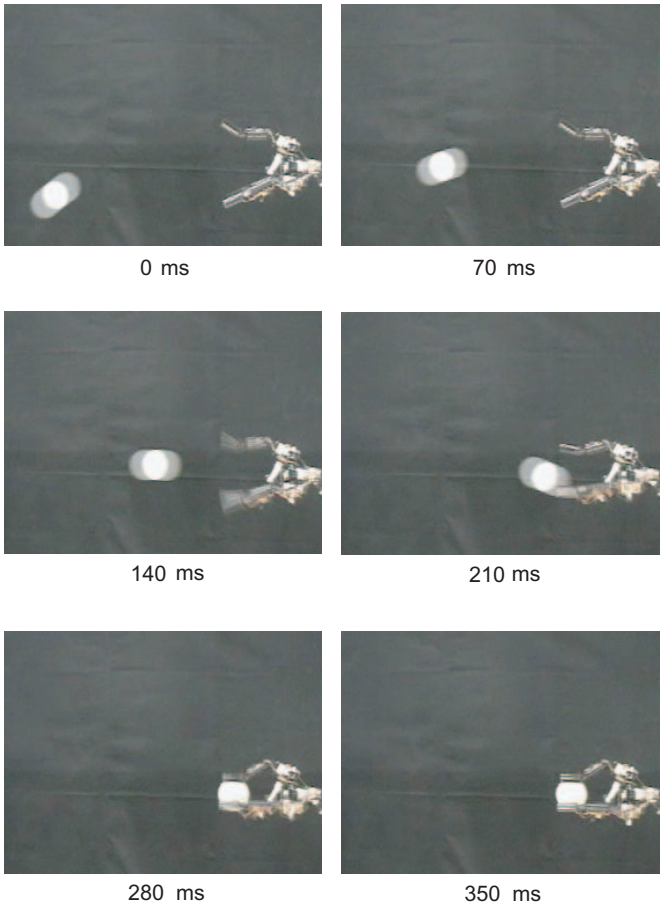

Fig. 13. Snapshots of catching motion

V. Conclusion

The present paper proposed the strategy for a robotic hand to catch a ball with the high manipulability grasp configuration in a vertical plane using a vision system. We verified experimentally its effectiveness using the NDA Hand, which had ability of the finger-thumb opposition and a high-speed performance. The strategy enables the robot to catch a moving object with the grasp configuration taking consideration of the following manipulation after the catching. Although its success rate is not high due to the deviation of the rubber-ball from the vertical plane, we consider that its success rate will be improved if the three-dimensional position of the object can be measured with two high-speed cameras.

In order to verify further advantages of the strategy, our future work attempts to realize the dynamic manipulation [5] by repeating grasp and release of the object such as a baton twirling.

Finally, we appreciate corporation of Harmonic Drive Systems Inc. and Hamamatsu Photonics K.K..

References

[1] A. Bicchi, C. Melchiorri and D. Balluchi: "On the Mobility and Manipulability of General Multiple Limb Robots," IEEE Trans. Robotics and Automation, Vol.11, No.2, pp.215-228, 1995.
[2] A.B.A Cole, J.E. Hauser, S.H. Sastry: "Kinematics and Control of Multifingered Hands with Rolling Contact," IEEE Trans. Automation Control, Vol.34, No.4, pp.398-404, 1989.
[3] W. Hong and J.E. Slotine: "Experiments in hand-eye coordination using active vision," Proc. 4th Int. Symp. on Experimental Robotics, 1995.
[4] M. Jeannerod: "The Timing of Natural Prehension Movements," J. of Motor Behavior, Vol.16, No.3, pp.235-254, 1984.
[5] M.T. Mason:"Mechanics of Robotic Manipulation," The MIT Press, 2001.
[6] A.T. Miller and P.K. Allen: "Grasp It - A Versatile Simulator for Robotic Grasping," IEEE Robotics and Automation Magazine, Vol.11, No.4, pp.110-122, 2004.
[7] J. Napier (revised by R.H. Tuttle): "Hands," Princeton Science Library, 1993.
[8] A. Namiki, Y. Imai, M. Ishikawa and M. Kaneko: "Development of a High-speed Multifingered Hand System and Its Application to Catching," Proc. IEEE Int. Conf. on Intelligent Robots and Systems (IROS), pp.2666-2671, 2003.
[9] N. Furukawa, A. Namiki, T. Senoo, M. Ishikawa: "Dynamic Regrasping Using a High-speed Multifingered Hand and a High-speed Vision System," Proc. IEEE Int. Conf. on Robotics and Automation (ICRA), pp.181-187. 2006.
[10] J.C. Trinkle: "On the Stability and Instantaneous Velocity of Grasped Frictionless Objects," IEEE Trans. Robotics and Automation, Vol.8, No.5, pp.560-572, 1992.
[11] M. Yashima and H. Yamaguchi: "Dynamic Motion Planning Whole Arm Grasp Systems Based on Switching Contact Modes," Proc. IEEE Int. Conf. on Robotics and Automation (ICRA), pp.2492-2499, 2002.

Appendix

From (2) and (3), we can get the following equations

$$\|\boldsymbol{V}_o\|^2 = \boldsymbol{z}^T \boldsymbol{C}_V^T \boldsymbol{C}_V \boldsymbol{z} \tag{7}$$

$$\|\dot{\boldsymbol{\theta}}\|^2 = \boldsymbol{z}^T \boldsymbol{C}_\theta^T \boldsymbol{C}_\theta \boldsymbol{z} \leq 1 \tag{8}$$

Assuming that the manipulation system is kinematically identical [11], which shows that the object velocity $\boldsymbol{V}_o$ is uniquely determined by the joint velocity $\dot{\boldsymbol{\theta}}$, the null space of the $\boldsymbol{C}_\theta$ does not exist. The matrix $\boldsymbol{C}_\theta^T \boldsymbol{C}_\theta$ becomes a positive definite symmetric matrix, which can be described as $\boldsymbol{C}_\theta^T \boldsymbol{C}_\theta = \boldsymbol{P}^T \boldsymbol{P}$ by a nonsingular matrix $\boldsymbol{P}$. Eqs. (7) and (8) can be rewritten by a new variable $\tilde{\boldsymbol{z}} = \boldsymbol{P}\boldsymbol{z}$, which are

$$\|\boldsymbol{V}_o\|^2 = \tilde{\boldsymbol{z}}^T \boldsymbol{P}^{-T} \boldsymbol{C}_V^T \boldsymbol{C}_V \boldsymbol{P}^{-1} \tilde{\boldsymbol{z}} \tag{9}$$

$$\|\dot{\boldsymbol{\theta}}\|^2 = \tilde{\boldsymbol{z}}^T \tilde{\boldsymbol{z}} \leq 1 \tag{10}$$

Since $\boldsymbol{Q} = \boldsymbol{P}^{-T} \boldsymbol{C}_V^T \boldsymbol{C}_V \boldsymbol{P}^{-1}$ is positive-semidefinite, the singular value decomposition of $\boldsymbol{Q}$ can be described as

$$\boldsymbol{Q} = \boldsymbol{U}_Q \boldsymbol{D}_Q {\boldsymbol{U}_Q}^T \tag{11}$$

where $\boldsymbol{U}_Q$ is an orthogonal matrix and the diagonal elements of $\boldsymbol{D}_Q = \mathrm{diag}(d_1, \cdots, d_q)$ are the eigenvalues of $\boldsymbol{Q}$.

Substituting (11) and a new variable $\bar{\boldsymbol{z}} = {\boldsymbol{U}_Q}^T \tilde{\boldsymbol{z}}$ into (9) and (10) finally yields

$$\begin{aligned} \|\boldsymbol{V}_o\|^2 &= \tilde{\boldsymbol{z}}^T (\boldsymbol{U}_Q \boldsymbol{D}_Q \boldsymbol{U}_Q^T) \tilde{\boldsymbol{z}} \\ &= \bar{\boldsymbol{z}}^T \boldsymbol{D}_Q \bar{\boldsymbol{z}} = d_1 \bar{z}_1^2 + d_2 \bar{z}_2^2 + \cdots + d_p \bar{z}_p^2 \\ \|\dot{\boldsymbol{\theta}}\|^2 &= \bar{\boldsymbol{z}}^T \bar{\boldsymbol{z}} \leq 1 \end{aligned}$$